Quasiparton distributions in massive QED2: Toward quantum computation

Sebastian Grieninger,[1,2,*] Kazuki Ikeda,[1,2,†] and Ismail Zahed[1,‡]

[1]*Center for Nuclear Theory, Department of Physics and Astronomy, Stony Brook University, Stony Brook, New York 11794–3800, USA*

[2]*Co-design Center for Quantum Advantage (C2QA), Stony Brook University, Stony Brook, New York 11794–3800, USA*

(Received 18 April 2024; accepted 16 September 2024; published 7 October 2024)

We analyze the quasiparton distributions of the lightest η' meson in massive two-dimensional quantum electrodynamics (QED2) by exact diagonalization. The Hamiltonian and boost operators are mapped onto spin qubits in a spatial lattice with open boundary conditions. The lowest excited state in the exact diagonalization is shown to interpolate continuously between an anomalous η' state at strong coupling, and a nonanomalous heavy meson at weak coupling, with a cusp at the critical point. The boosted η' state follows relativistic kinematics but with large deviations in the luminal limit. The spatial quasiparton distribution function and amplitude for the η' state are computed numerically for increasing rapidity both at strong and weak coupling, and compared to the exact light front results. The numerical results from the boosted form of the spatial parton distributions, compare fairly with the inverse Fourier transformation of the luminal parton distributions, derived in the lowest Fock space approximation. Our analysis points out some of the limitations facing the current lattice program for the parton distributions.

DOI: 10.1103/PhysRevD.110.076008

I. INTRODUCTION

Light cone distributions play a central role in the evaluation of hard inclusive and exclusive processes in quantum chromodynamics (QCD). Whenever factorization holds, a hard process is amenable to a perturbative contribution times pertinent parton distributions or fragmentation functions, e.g. Drell-Yan and jet processes. Accurate light cone distribution functions are essential for the analyses of many of the semi-inclusive processes being carried at the current JLAB facility, and planned at the future EIC [1,2].

The parton distribution functions are valued on the light front and inherently nonperturbative, which make them inaccessible to standard Euclidean lattice formulations, except through few lowest moments. This major shortcoming has been circumvented by Ji's proposal [3], through the use of quasiparton distributions. The leading twist light front partonic correlators are traded for equal-time correlators in increasingly boosted hadronic states, which are then matched perturbatively on the light cone [4–9].

The quasiparton distribution matrix elements calculated in a fixed size Euclidean lattice QCD have been shown to match those obtained through LSZ reduction in continuum Minkowski QCD to all orders in perturbation theory [10]. Some variants of this formulation have also been proposed as pseudo distributions [11] and lattice cross sections [12]. Recently, an increasing number of QCD lattice collaborations have implemented some of these ideas and succeeded in numerically extracting the light cone parton distributions, modulo the shortcomings inherent to a finite lattice.

To understand some of these shortcomings, quasiparton distribution functions have been analyzed in two-dimensional QCD in leading and next-to-leading contributions in the large N_c limit [13]. The results confirm the soundness of the approach, away from the critical regions in parton-x $x = 0,\ 1$, where the method breaks down. In this work, we would like to revisit the analysis of the quasiparton distributions in two-dimensional massive QED utilizing a spin formulation of the lattice Schwinger model and solving it by exact diagonalization as an exploratory study for a future quantum computation. The purpose is to understand the feasibility and numerical issues that follow from this digitization. We note that a similar approach has been recently carried for the parton distributions for a schematic Nambu-Jona-Lasinio (NJL) model in two-dimensions [14,15]. In the context of quantum computations, partonic observables were previously considered in [16–18]. Finally, simulating quantum field theories in the light-front formulation on quantum computers was explored in [19,20].

*Contact author: sebastian.grieninger@stonybrook.edu
†Contact author: kazuki.ikeda@stonybrook.edu
‡Contact author: ismail.zahed@stonybrook.edu

In this work massive QED2 is formulated on a spatial lattice with continuous time, using Kogut-Suskind fermions [21,22]. The fermion fields are eliminated with the help of a Jordan-Wigner transformation [23]. While these procedures are by now standard, their application to understand the partonic content of physical states in a gauge theory with massive QED2 as a protype, is new. More specifically, our paper contains a number of new results: (1) We show anew the central role played by the boost operator in the analysis of the light front wave functions in real time; (2) We show anew how the low-lying physical spectrum of a gauge theory transforms under increasing boosts, with a quantitative description of the numerical limitations in the luminal limit in QED2; (3) We provide a new Hamiltonian formulation to the concept of quasi-PDFs in real-time, in a gauge theory with QED2 as an example; (4) We use the qubit form of the QED2 Hamiltonian and boost operators to extract anew the spatial quasidistributions in QED2 in real time, and study their dependence on the boost transformation with a comparison to the expected exact results. These are essential new theoretical steps and checks, to enforce in any attempt on the road towards quantum computation of partonic distributions in hadronic physics.

Quantum computing and quantum simulation offer unique capabilities that vastly surpass what classical computation alone can achieve, particularly in addressing specific challenges in nuclear physics [24]. A key challenge in quantum simulation/computation of gauge theories, is a scalability of the system size. The ground state of general one-dimensional spin chains can be solved using the matrix product state (MPS) approximation [25–27], which underlines the density matrix renormalization group (DMRG) [28,29] algorithm. A number of challenging properties of the ground state of the Schwinger model have been studied with quantum computers [30,31] and simulators [32] for a large number of qubits (up to hundreds qubits). However, the nontrivial dynamics of the excited states has received less attention, although some basic properties of the first excited state were studied [33,34]. To open a new directional study in massive QED2, as a testing ground for four-dimensional QCD, we will focus on the boosted properties of the first excited state and its partonic content. Our results will provide interesting and important benchmarks towards a quantum computation in QCD. Moreover our setup can be extended to a large system size by using more advanced MPS methods, to approximate the excited states [34,35].

The outline of the paper is as follows: in Sec. II, we briefly review the general features of the strong and weak coupling regime of massive QED2. In Sec. III, we recall the light front equation for the lowest meson state in the lowest Fock state approximation, and its solutions. In Sec. IV, we introduce the boost operator, and map massive QED2 including the boost operator onto a spin system using standard techniques. A detailed analysis of the deviation from the luminal limit for the boosted state is given. We also show how the boost operator can be traded for a "time" evolved spatial correlator directly on the light front in the luminal case. In Sec. V, we detail the numerical results for the parton distribution functions and amplitudes obtained from the exact diagonalization, using the boosted as well as the "time" evolved forms, both for strong and weak coupling. The results are compared to the exact continuum result. Our conclusions are in Sec. VI.

II. MASSIVE QED2

The two-dimensional quantum electrodynamics (QED2), also known as the Schwinger model [36], exhibits a variety of nonperturbative phenomena familiar from four-dimensional gauge theories. The extensive interest in QED2 stems from the fact that it bears much in common with two-dimensional QCD since the Coulomb law is confining in two dimensions. As a result, the QED2 spectrum involves only chargeless excitations. Remarkably, the vacuum state is characterized by a nontrivial chiral condensate and topologically active tunneling configurations.

QED2 with massive fermions is described by [36,37]

$$S=\int d^2x\left(\frac{1}{4}F_{\mu\nu}^2+\frac{\theta\tilde{F}}{2\pi}+\bar{\psi}(i\not{D}-m)\psi\right), \tag{1}$$

with $\not{D}=\not{\partial}-ig\not{A}$. The bare fermion mass is m and the coupling g has mass dimension. At weak coupling with $m/g>1/\pi$, the spectrum is composed of heavy mesons, with doubly degenerate C-even and C-odd vacuua at $\theta=\pi$. At strong coupling with $m/g<1/\pi$, the spectrum is composed of light mesons and baryons, with a C-even vacuum whatever θ. More specifically:

Strong coupling $\frac{m}{g}\ll\frac{1}{\pi}$: The squared rest mass is

$$m_\eta^2=m_S^2+m_\pi^2=\frac{g^2}{\pi}-\frac{m\langle\bar{\psi}\psi\rangle_0}{f^2}, \tag{2}$$

with $f=1/\sqrt{4\pi}$ the η' decay constant [38]. The vacuum chiral condensate is finite in the chiral limit with $\langle\bar{\psi}\psi\rangle_0=-\frac{e^{\gamma_E}}{2\pi}m_s$ [39,40], where $\gamma_E=0.577$ is Euler constant. Hence,

$$\frac{m_\eta}{m_s}=\left(1+2e^{\gamma_E}\frac{m}{m_s}\right)^{\frac{1}{2}}\approx 1+e^{\gamma_E}\frac{m}{m_s}, \tag{3}$$

in the strong coupling regime.

Weak coupling $\frac{m}{g}\gg\frac{1}{\pi}$: The η-mass is expected to asymptote $m_\eta\to 2m$. Note that at weak coupling (3) we have $e^{\gamma_E}\approx 1.78$ which is close to 2, hence allowing a smooth and continuous transition in the eta mass from weak to strong coupling.

III. LIGHT FRONT WAVE FUNCTIONS

Modulo the U(1) anomaly, the light front Hamiltonian associated with QED2 is very similar to QCD2. Massless QED2 is exactly solvable with a single bosonic excitation of mass m_s in the spectrum. On the contrary, massive QED2 is not exactly solvable, and is characterized by multiboson states.

In the 2-particle Fock approximation, massless QED2 admits a ground state and a tower of spurious states that disappear in the continuum when higher Fock states contributions are included [41]. Massive QED2 in the 2-particle Fock space approximation admits a ground state and a tower of multimeson states that are not spurious. The ground state is largely a 2-particle Fock contribution while the first excited state already contains a large 4-particle Fock space contribution (meson-meson bound state) [42].

With this in mind, the light front wave functions $\varphi_n(\zeta)$ in the 2-particle Fock-space approximation follow from a similar Bethe-Salpeter derivation. More specifically, the light front wave functions solve [41]

$$M_n^2\varphi_n(\zeta) = \frac{1}{2}m_s^2\int_{-1}^{1}d\zeta'\varphi_n(\zeta') + \frac{4m^2}{1-\zeta^2}\varphi_n(\zeta) - 2m_s^2\mathrm{PP}\int_{-1}^{1}d\zeta'\frac{\varphi_n(\zeta')-\varphi_n(\zeta)}{(\zeta'-\zeta)^2}, \tag{4}$$

with ζP the symmetric momentum fraction of the partons. Here PP is short for the principal part. Equation (4) is the 't Hooft equation [43], modulo the U(1) anomaly contribution (first term on the right-hand side). The longitudinal kinetic contribution (second term on the right-hand side) is singular at $\zeta = \pm 1$, forcing the light front wave function to vanish at the edges $\varphi_n(\pm 1) = 0$. Note that the 2-particle Fock-contribution is the leading contribution in the limit of a large number of colors in QCD2.

In the massless limit with $m \to 0$, the spectrum is that of a single massive boson,

$$\varphi_\eta(\zeta) = \varphi_0(\zeta) \to \frac{1}{\sqrt{2}}\theta(1-\zeta^2), \qquad M_0^2 \to m_s^2. \tag{5}$$

For small m, the lowest solution vanishes at the end points as powers of m,

$$\varphi_\eta(x) = \frac{C_\eta}{f}(1-\zeta^2)^\beta \tag{6}$$

with β fixed by [43]

$$\frac{m^2}{m_s^2} = 1 - \pi\beta\cot(\pi\beta). \tag{7}$$

In the massive limit with $m \gg m_s$, the solution is peaked around $x = \frac{1}{2}$, with $M \approx 2m$.

In general, (4) admits a tower of excited states for finite m/m_s since the PP part in (4) is strictly confining. They are given semiclassically by

$$\varphi_n(x) = \sqrt{2}\sin\left((n+1)(1+\zeta)\frac{\pi}{2}\right). \tag{8}$$

Because of screening, which is not suppressed in massive QED2, the excited mesons states decay whenever $M_n > 2M_0$. The lowest state parton distribution function is of the form,

$$q_\eta(\zeta) = \mathrm{sgn}(\zeta)|\varphi_\eta(|\zeta|)|^2. \tag{9}$$

with $\mathrm{sgn}(\zeta)$ the signum function. Since η' is flavor neutral, the fermion and antifermion distribution functions are identical.

The integral equation (4) is a relative of the 't Hooft equation and can be solved by variational or other numerical methods. Here, we use a direct discretization into an matrix eigenvalue equation as for the 't Hooft equation [44]. For that we define the rescaled masses,

$$\mu^2 = M^2/m_s^2 \qquad \alpha = m^2/m_s^2,$$

so that (4) reads

$$\mu^2\varphi(\zeta) = \frac{1}{2}\int_{-1}^{1}d\zeta'\,\varphi(\zeta') + \frac{4\alpha}{1-\zeta^2}\varphi(\zeta) - 2\mathrm{PP}\int_{-1}^{1}d\zeta'\frac{\varphi(\zeta')-\varphi(\zeta)}{(\zeta-\zeta')^2}, \tag{10}$$

subject to the end point conditions $\varphi(\pm 1) = 0$. The solutions follow numerically by expanding in a complete basis, the details of which are summarized in Appendix A. A more standard but straightforward x-representation is summarized in Appendix B.

In Fig. 1 we show typical solutions in the strong and weak coupling regimes. We will refer to these solutions as

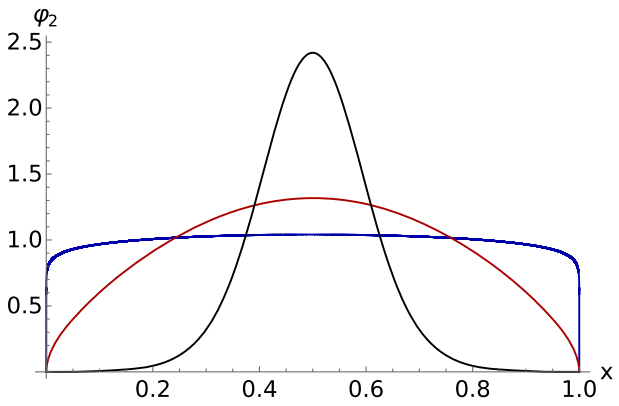

FIG. 1. Solution to (B1) for $\beta = 0.1\sqrt{3}/\pi$ (blue), $\beta = \sqrt{3}/\pi$ (red), $\beta = 10\sqrt{3}/\pi$ (black) using 13 Jacobi polynomials.

"exact solution" even though the solutions are approximated, in the sense that we cut the expansion in the Jacobi basis at a finite number of Jacobi polynomials. However, higher Jacobi polynomials are rapidly suppressed.

IV. BOOSTED QUASIPARTONIC FUNCTIONS

To quantify the partonic distributions in the lowest meson η' in massive QED2, we will make use of the appropriate Ji's quasidistributions [3], in a boosted state. This construction allows for testing the numerical limitations when addressing the ultra-relativistic and large spatial volume limits. We will present two equivalent forms of the quasidistribution functions, one using explicitly the boost operator and the other trading it for the "time" evolved operator.

A. Boost operator in QED2

For $\theta = 0$ and in the temporal gauge $A^0 = 0$, the Hamiltonian and boost operators associated to (1) read

$$\mathbb{H} = \int dx \left(\frac{1}{2} E^2 + \psi^\dagger (i\alpha D_x + m\gamma^0)\psi \right),$$
$$\mathbb{K} = \int dx x \left(\frac{1}{2} E^2 + \psi^\dagger (i\alpha D_x + m\gamma^0)\psi \right). \tag{11}$$

Note that both operators develop CP odd contributions under the substitution $m \to m e^{i\gamma^5\theta}$ for a finite vacuum angle. The operators (11) satisfy the Poincare algebra,

$$[\mathbb{K}, \mathbb{H}] = i\mathbb{P}, \tag{12}$$

$$[\mathbb{K}, \mathbb{P}] = i\mathbb{H}, \tag{13}$$

with the momentum operator $\mathbb{P}$.

Physically boosted states are defined as

$$|\eta(\chi)\rangle = e^{i\chi\mathbb{K}} |\eta(0)\rangle, \tag{14}$$

with χ the rapidity in the x-direction,

$$\chi = \frac{1}{2} \ln \left(\frac{1+v}{1-v} \right). \tag{15}$$

If η' is the lowest massive meson in the spectrum at strong coupling, with rest mass (normal ordering assumed),

$$:\mathbb{H}: |\eta(0)\rangle = m_\eta |\eta(0)\rangle, \tag{16}$$

then the boosted state is relativistic,

$$:\mathbb{H}: |\eta(\chi)\rangle = m_\eta \cosh\chi |\eta(\chi)\rangle,$$
$$:\mathbb{P}: |\eta(\chi)\rangle = m_\eta \sinh\chi |\eta(\chi)\rangle, \tag{17}$$

with four-momentum $p^\mu = \gamma m_\eta (1, v)$, and $\gamma = \cosh\chi = 1/\sqrt{1-v^2}$. Note that on the light cone

$$P^\pm = \frac{1}{\sqrt{2}} \gamma m_\eta (1 \pm v) = \frac{1}{\sqrt{2}} m_\eta e^{\pm\chi}.$$

B. Boosted quasidistributions

With this in mind, we define the distribution amplitude for the boosted η' meson as

$$\varphi_\eta(x, v) = \frac{1}{2if} \int_{-\infty}^{+\infty} \frac{dz}{2\pi} e^{-iz\zeta p^1} \langle 0|\bar\psi(0, -z)[-z, +z]_S \times \gamma^+\gamma^5 \psi(0, +z) e^{i\chi\mathbb{K}} |\eta(0)\rangle, \tag{18}$$

with $p^1 = \gamma m_\eta v$ and $\zeta = 2x - 1$ with x the parton fraction. The link variable $[-z, +z]_S$ is along the spatial direction, and $f = 1/\sqrt{4\pi}$ the two-dimensional eta decay constant. Here $\gamma^+ = \gamma^0 + \gamma^1$, $\gamma^5 = \gamma^0\gamma^1$, with $\gamma^0 = \sigma^3$ and $\gamma^1 = i\sigma^2$. Note that in two-dimensions $\bar\psi\gamma^+\psi = \bar\psi\gamma^+\gamma^5\psi$. Similarly, the partonic distribution function is defined as

$$q_\eta(x, v) = \frac{1}{2} \int_{-\infty}^{+\infty} \frac{dz}{2\pi} e^{-iz\zeta p^1} \langle \eta(0)|e^{-i\chi\mathbb{K}} \bar\psi(0, -z)[-z, +z]_S \times \gamma^+\gamma^5 \psi(0, +z) e^{i\chi\mathbb{K}} |\eta(0)\rangle. \tag{19}$$

Here (18) and (19) are partonic functions defined at equal time for a fixed boost, which reduce to the light front partonic functions in the large rapidity limit $\chi \gg 1$. They are Ji's quasipartonic functions and therefore have support on [0, 1] only in the large rapidity limit. Note that both (18) and (19) normalize to 1 in this limit.

C. "Time" evolved quasidistributions

The boost operator in the quasidistribution, can be traded for a Hamiltonian evolution. In the luminal case, it reduces to a direct evaluation of the parton distribution functions on the light front with Minkowski signature. This is possible since QED2 is UV finite. To show this, we use the boost identities,

$$e^{-i\chi\mathbb{K}} \psi(0, +z) e^{i\chi\mathbb{K}} = S[v]\psi(-\gamma v z, +\gamma z),$$
$$e^{-i\chi\mathbb{K}} \bar\psi(0, -z) e^{i\chi\mathbb{K}} = \bar\psi(+\gamma v z, -\gamma z) S[v]^{-1}, \tag{20}$$

with $S[v] = e^{\frac{1}{2}\chi\gamma^5}$. Inserting (20) into (18) yields

$$\varphi_\eta(x, v) = \frac{1}{2if} \int_{-\infty}^{+\infty} \frac{dz}{2\pi} e^{-iz\zeta m_\eta v} \langle 0|\bar\psi(+vz, -z)[-z, +z]_L \times \Gamma_v \psi(-vz, +z)|\eta(0)\rangle, \tag{21}$$

after a shift $\gamma z \to z$ with $\Gamma_v = -(\gamma^- + v\gamma^+)$ and the gauge link $[-z, +z]_L$ is now along the light cone. Note that the

standard spin source $\Gamma_v \to \gamma^+$ in (21) is obtained by using $\gamma^+\gamma^5 \to \gamma^0$ in (18). We have traded the boosted η' state for a fermionic bi-local correlator with light cone support for $v \to 1$. In this limit, Ji's quasidistribution is the light-front distribution for the η' meson, expressed in the η' rest frame, for both choices of Γ_v quoted. No matching is required since massive QED2 is finite in the UV modulo normal ordering. Also note that the boost transformation turns the spatial gauge link lightlike at the end points.

Using the "time" identities,

$$\begin{aligned}\psi(-vz,+z) &= e^{-ivz\mathbb{H}}\psi(0,+z)e^{+ivz\mathbb{H}},\\ \bar{\psi}(+vz,-z) &= e^{+ivz\mathbb{H}}\psi(0,-z)e^{-ivz\mathbb{H}},\end{aligned} \tag{22}$$

we can recast (21) as

$$\begin{aligned}\varphi_\eta(x,v) = \frac{1}{2if}\int_{-\infty}^{+\infty}\frac{dz}{2\pi}e^{-iz(\zeta-1)m_\eta v}\langle 0|\bar{\psi}(0,-z)[-z,+z]_L\\ \times\Gamma_v e^{-i2vz\mathbb{H}}\psi(0,+z)|\eta(0)\rangle.\end{aligned} \tag{23}$$

The boost operator in (21) has been traded for the real "time evolution operator," albeit with the effective "time" of $t_z = 2vz$. A rerun of the same arguments for the parton distribution function (19), yields

$$\begin{aligned}q_\eta(x,v) = \frac{1}{2}\int_{-\infty}^{+\infty}\frac{dz}{2\pi}e^{-iz\zeta m_\eta v}\langle\eta(0)|\bar{\psi}(0,-z)[-z,+z]_L\\ \times\Gamma_v e^{-i2vz\mathbb{H}}\psi(0,+z)|\eta(0)\rangle,\end{aligned} \tag{24}$$

with the normalization,

$$\int_0^1 dx\, p_\eta(x,v) = 1.$$

This "time" evolved form for $v = 1$ was noted in [14,15]. The advantage of (23) and (24) over (21), is their manifest finiteness as $v \to 1$. Below, we will use the digitalization of both (21) and (23) and (24) for a cross check on their accuracy on a finite grid of qubits.

V. LATTICIZED KOGUT-SUSSKIND HAMILTONIAN

We will map our Hamiltonian onto a lattice spin system of length $L = Na$ to make it suitable for exact diagonalization. Using staggered fermions, the map for the two-dimensional massive Schwinger model and gauge fixing using Gauss law is standard [45]. Here, we only detail the mapping of the boost operator for completeness. Throughout the work, we obtained the excited states by exact-diagonalization of the Hamiltonian (31). One can implement such excited states on a quantum computer by using a variational quantum deflation (VQD) algorithm [46].

A. Digitized boost operator

More specifically, the gauge field contribution to the boost operator is

$$\mathbb{K}_G = \frac{1}{2}g^2 a\sum_{n=0}^{N-1} nL_n^2, \tag{25}$$

where L_n are link operators [45]. Each staggered Dirac fermion at site n is assigned a bispinor with upper component on even sites, and lower component on odd sites,

$$\psi(0,z=na) = \frac{1}{\sqrt{a}}\begin{pmatrix}\psi_e(n)\\ \psi_o(n)\end{pmatrix} = \frac{1}{\sqrt{a}}\begin{pmatrix}\varphi_{n:\text{even}}\\ \varphi_{n+1:\text{odd}}\end{pmatrix}, \tag{26}$$

with $0 \le n \le N-1$. The massive staggered fermion contribution to the boost operator is

$$\mathbb{K}_F = \frac{1}{2}\sum_{n=0}^{N-1} in\left(\varphi_n^\dagger\varphi_{n+1} - \varphi_{n+1}^\dagger\varphi_n\right) + ma\sum_{n=0}^{N-1}(-1)^n n\varphi_n^\dagger\varphi_n. \tag{27}$$

Fermion bilocals with the gauge link set to 1 (in two-dimensions the gauge field can be eliminated by fixing the gauge and resolving Gauss law), are digitized as

$$\begin{aligned}&\bar{\psi}(0,-z)(\gamma^0+\gamma^1)\gamma^5\psi(0,+z)\\ &\quad= \frac{1}{a}\left(\psi_e^\dagger(-n)+\psi_o^\dagger(-n)\right)\left(\psi_e(+n)+\psi_o(+n)\right).\end{aligned} \tag{28}$$

The chiral fermions map onto $\psi_e(n) = \varphi_n$ (even sites) and $\psi_o(n) = \varphi_n$ (odd sites) with [21–23,45]

$$\begin{aligned}\varphi_n &= \prod_{m<n}[+iZ_m]\frac{1}{2}(X_n - iY_n),\\ \varphi_n^\dagger &= \prod_{m<n}[-iZ_m]\frac{1}{2}(X_n + iY_n).\end{aligned} \tag{29}$$

The full boost operator maps onto

$$\begin{aligned}\mathbb{K} \to \frac{1}{2}g^2 a\sum_{n=0}^{N-1} nL_n^2 + \frac{1}{4}\sum_{n=0}^{N-1} n(X_nX_{n+1} + Y_nY_{n+1})\\ + \frac{ma}{2}\sum_{n=0}^{N-1}(-1)^n n(1+Z_n),\end{aligned} \tag{30}$$

and the Hamiltonian maps onto [47–52]

$$\begin{aligned}\mathbb{H} \to \frac{1}{4a}\sum_{n=1}^{N-1}\left(X_nX_{n+1} + Y_nY_{n+1}\right)\\ + \frac{m}{2}\sum_{n=1}^{N}(-1)^n Z_n + \frac{ag^2}{2}\sum_{n=1}^{N-1}L_n^2,\end{aligned} \tag{31}$$

where L_n is the local electric field operator,

$$L_n = \sum_{j=1}^{n} \frac{Z_j + (-1)^j}{2}. \tag{32}$$

B. Digitized boosted η'-state

The discrete lattice version of the boost operator can be tested on the η' state at rest to quantify the numerical deviations from the relativistic result in the continuum. For that, we start by setting the scale $g = 1$, and recording all other scales in units of g. For now, we fix the number of qubits $N = 20$ with a spatial lattice spacing $a = 1$. For better numerical accuracy in the Schwinger model, we follow [53] and evaluate the expressions as a function of the improved mass,

$$m_{\text{lat}} = m - \frac{1}{8} g^2 a \to m - \frac{1}{8}. \tag{33}$$

The mass gap in a finite spatial box of length $L = Na \to N$, receives finite size corrections $E_0 = \sqrt{m_s^2 + \pi^2/L^2}$ with $L = N \cdot a$, with $m_s^2 = g^2/\pi \to 1/\pi$.

In Fig. 2 we show the behavior of the physical mass gap at rest, as a function of the improved current mass m/g. The red-dashed line (left) is a fit to

$$\frac{E}{E_0} = 0.99 + 1.76 \frac{m}{E_0}, \tag{34}$$

and the green-dashed line in the inset (left), is a fit to

$$\frac{E}{E_0} = \frac{0.33 + 1.99m}{E_0}. \tag{35}$$

In the inset, a clear crossing from strong to weak coupling at about $m/g \sim 1/3$ is observed, which is consistent with expectations $m/g \approx 1/\pi$ (critical point). The lightest η' state

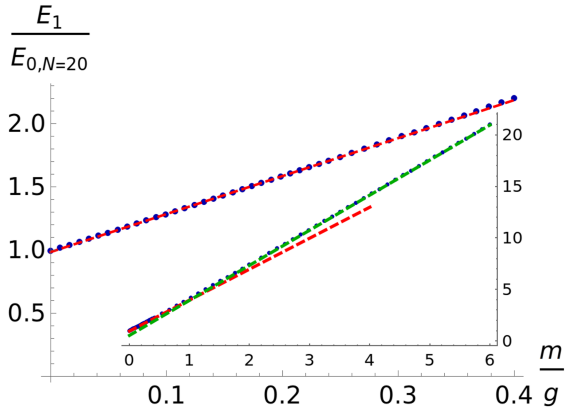

FIG. 2. Normalized mass gap as a function of the improved mass m_{lat} with $g = a = 1$ and $N = 20$. The red-dashed line is a fit to (34) and the green-dashed line in the inset is a fit to (35).

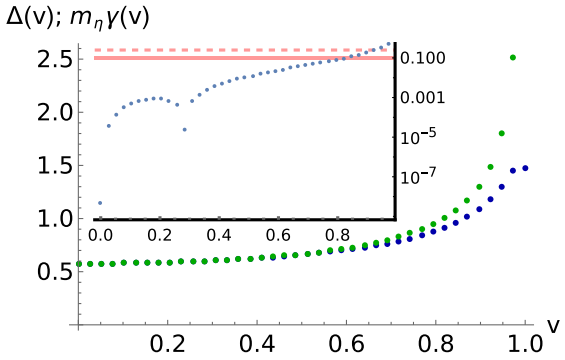

FIG. 3. Relativistic dispersion of the η' state in dotted-blue (exact diagonalization) and in dotted-green (exact). We fixed $N = 24$ and the improved mass as $m_{\text{lat}} = -0.125g^2a$ ($a = 1 = g$). The symmetric relative error is shown in the inset in dotted-blue. The red line indicates an error in excess of 10% (at around $v \gtrsim 0.83$), while the dashed-red line implies an error in excess of 20% (at around $v \gtrsim 0.91$).

in the spectrum is gapped by $m_s/E_0 \sim 1$ for zero current mass in the strong coupling regime, and asymptotes the nonrelativistic limit of $2m/E_0 \sim 2m/m_s$ in the weak coupling regime.

Here we emphasize that the spectrum of $:\mathbb{H}:$ following by exact diagonalization exhibits numerous spurious states, which are eliminated by imposing Gauss's law, i.e. zero electric charge. More specifically, the charge operator is given by

$$Q = \sum_{n=1}^{N} \frac{Z_n}{2}, \tag{36}$$

and the physical eigenstates are selected by the condition $\langle E_n|Q|E_n\rangle = 0$. Only when this condition is enforced, we see the physical crossover reported in Fig. 2.

In Fig. 3, we show the relativistic dispersion relation of boosted state obtained by exact diagonalization (dotted-blue) and the continuum relativistic result $p^1(v)$ (dotted-green), versus the velocity v for $N = 24$. The symmetric relative error is shown in the inset in dotted-blue, where the red line indicates that it exceeds 10% (at around $v \gtrsim 0.83$) and the dashed-red line that it exceeds 20% (at around $v \gtrsim 0.91$). Moreover, increasing the mass means that the symmetric error increases faster with v. The orthonormality of the ground state with the boosted η' state is only enforced for low velocities as illustrated in Fig. 4 (blue circles).

VI. PARTONIC FUNCTIONS FROM EXACT DIAGONALIZATION

In this section, we will perform a numerical analysis of the quasi-parton distributions in QED2 obtained by exact diagonalization as a testing ground for a future quantum simulations. In particular, we will carry out the analysis for both the boosted form and the "time" evolved form,

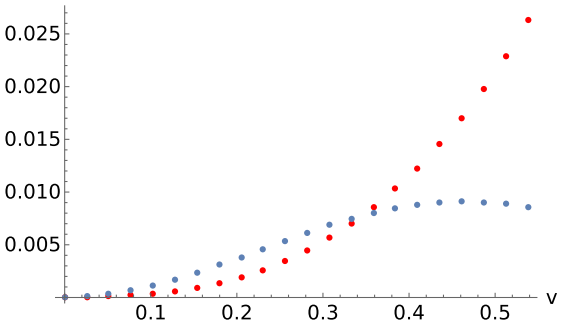

FIG. 4. Symmetric relative error of the boost (red dots) and $\langle\eta(0)|0(v)\rangle$ (blue dots) for $N=24$ and $m_{\rm lat}=0.1/\sqrt{\pi}-0.125g^2a(a=g=1)$.

to check both methods for consistency. For accuracy, the numerical results will be checked against the exact partonic distributions in the 2-parton Fock space approximation, derived earlier.

A. Boosted form

Using the symmetric forms (18) and (19), the mapped partonic distributions are

$$\begin{aligned}\varphi_\eta(\zeta,v)\to&\frac{a}{4\pi if}\sum_z e^{-iz\zeta P(v)}\langle 0|(\psi_e^\dagger(-z)+\psi_o^\dagger(-z))\\&\times(\psi_e(+z)+\psi_o(+z))e^{i\chi(v)\mathbb{K}}|\eta(0)\rangle\\=&\frac{1}{2\pi if}\sum_{n=\text{even}}e^{-in\zeta aP(v)}\langle 0|(\varphi_{-n}^\dagger+\varphi_{-n+1}^\dagger)\\&\times(\varphi_{+n}+\varphi_{+n+1})e^{i\chi(v)\mathbb{K}}|\eta(0)\rangle\\\equiv&\frac{1}{2\pi}\sum_{n=\text{even}}e^{-in\zeta aP(v)}\varphi(na),\end{aligned}\tag{37}$$

and

$$\begin{aligned}q_\eta(\zeta,v)\to&\frac{a}{4\pi}\sum_z e^{-iz\zeta P(v)}\langle\eta(0)|e^{-i\chi(v)\mathbb{K}}(\psi_e^\dagger(-z)+\psi_o^\dagger(-z))\\&\times(\psi_e(+z)+\psi_o(+z))e^{i\chi(v)\mathbb{K}}|\eta(0)\rangle\\=&\frac{1}{2\pi}\sum_{n=\text{even}}e^{-in\zeta aP(v)}\langle\eta(0)|e^{-i\chi(v)\mathbb{K}}(\varphi_{-n}^\dagger+\varphi_{-n+1}^\dagger)\\&\times(\varphi_{+n}+\varphi_{+n+1})e^{i\chi(v)\mathbb{K}}|\eta(0)\rangle\\\equiv&\frac{1}{2\pi}\sum_{n=\text{even}}e^{-in\zeta aP(v)}D(na),\end{aligned}\tag{38}$$

with $\zeta=2x-1$. The rest state $|\eta(0)\rangle$ is defined as an eigenstate of $:\mathbb{H}:$ of lowest mass modulo an arbitrary phase. This phase drops out in case of the distribution function, but does not in the distribution amplitude, so we set it to 1 in the latter to enforce real positivity.

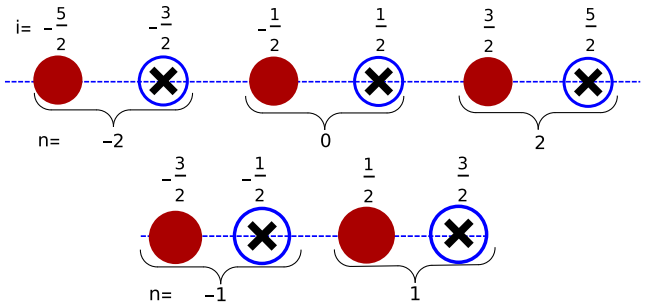

FIG. 5. Configuration of the staggered fermions for $N/2$ odd (upper plot for $N=6$) and $N/2$ even (lower plot for $N=4$). To compute the correlation functions such as (38), we symmetrically pair the first underbracket with the last, the second with the second to last etc.

Note that the spatial gauge links in (39) and (38) are reabsorbed into the site fermions, through the time-independent residual gauge transformation used in mapping the Hamiltonian to its spin form (31). In $1+1$ dimensions with open boundary conditions, both the electric flux and the vector potential can be eliminated, by explicitly solving Gauss' law and making use of the residual time-independent gauge transformation (modulo the flux at the left end point which we have set to 0).

In Fig. 6 (left-panel) we show the numerical results for the real and imaginary part of the spatial quasidistribution function $D(z)$ obtained from exact diagonalization, which enters the quasi-parton distribution function in (38). We use the lattice configuration illustrated in Fig. 5. The velocity is fixed to $v=0.925$ with the current mass $m/m_s=0.1$ (red disks) and with $m_{\rm lat}$ from (33) (blue triangles), both in the weak coupling regime. The numerical results hover around zero. The inverse Fourier transformation of the exact result following from (B1) is shown for $m/m_s=0.1$ (black-solid line) and for $m_{\rm lat}$ from (33) (black-dashed line). The solid curve is normalized to the peak value of the real part. We fixed $N=24$ with $a=g=1$.

In Fig. 6 (right-panel), we show also the real and imaginary part of the spatial distribution of $D(z)$ for $m/m_s=0.806$ (black-dashed line) in the weak coupling regime for $N=24$ with $a=g=1$. We again fixed the black lines to the peak of the real part at $z=0$.

Finally, we note that the limited number of qubits does not allow for an approximate fit of the parton distribution function in QED2, to the inverse Fourier transform of the 2-parameter ansatz $x^\alpha(1-x)^\beta$. This procedure is commonly used in the reconstruction of the parton distributions from the spatial distributions, in current lattice simulations [8].

B. "Time" evolved form

Using the symmetric forms (23) and (24) with $\Gamma_v\to\gamma^+$, the mapped partonic distributions are

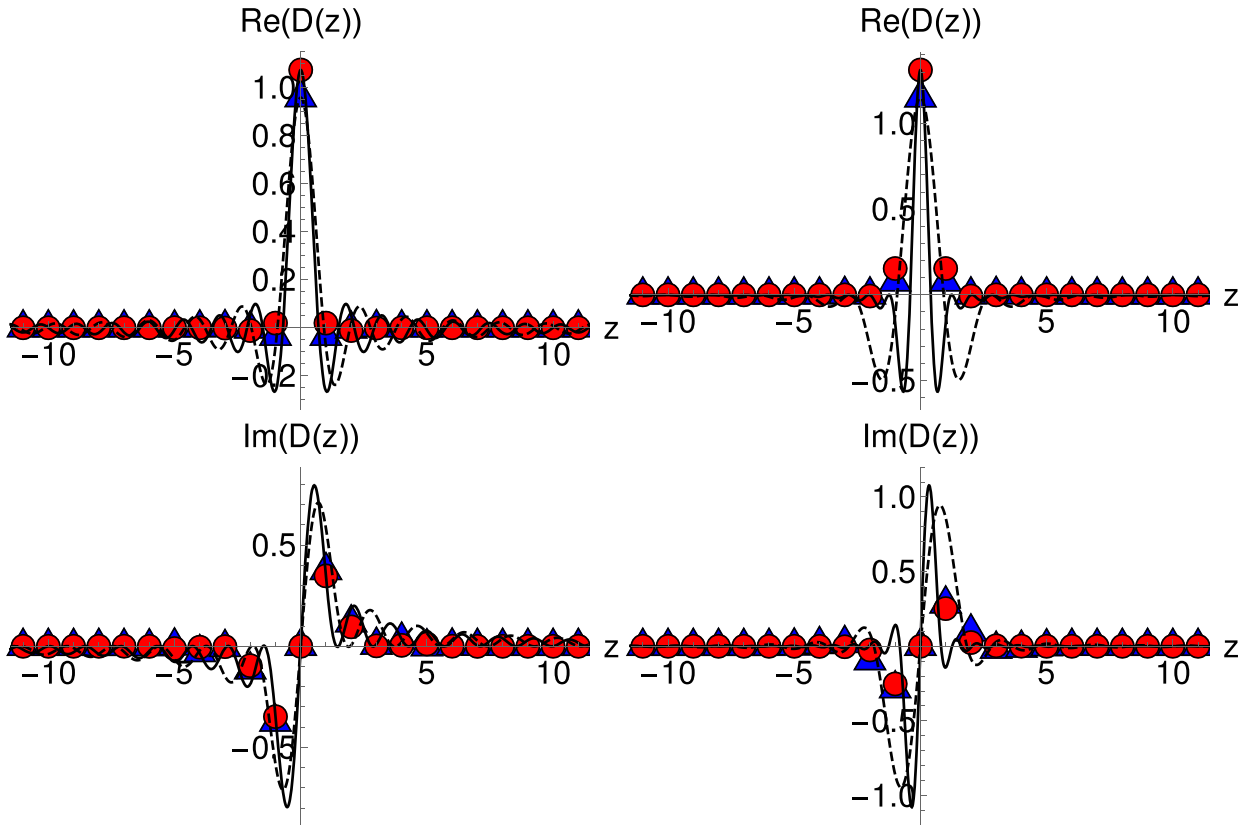

FIG. 6. *Left panel*: Real and Imaginary part of the spatial quasi-distribution function $D(z)$ for $v = 0.925$ and $m/m_s = 0.1$ (red disks) and the improved mass $m_{\rm lat}$ (blue triangles), both in strong coupling. The exact result following from (B1) by an inverse Fourier transform is shown for $m/m_s = 0.1$ (black-solid line) and the improved mass $m_{\rm lat}$ (33) (black-dashed line). We normalized the black curves to the peak of the real part, and fixed $N = 24$, with $a = g = 1$. *Right panel*: Same as the left panel but in the weak coupling regime for the improved mass $m/m_s = 0.806$.

$$\begin{aligned}\varphi_\eta(x,v) &\to \frac{a}{4\pi i f}\sum_z e^{-iz(\zeta-1)m_\eta v}\langle 0|(\psi_e^\dagger(-z)+\psi_o^\dagger(-z))e^{-i2vz\mathbb{H}}(\psi_e(+z)+\psi_o(+z))|\eta(0)\rangle \\ &= \frac{1}{2\pi i f}\sum_{n=\text{even}} e^{-\text{in}(\zeta-1)am_\eta v}\langle 0|(\varphi_{-n}^\dagger+\varphi_{-n+1}^\dagger)e^{-i2vn\mathbb{H}}(\varphi_{+n}+\varphi_{+n+1})|\eta(0)\rangle \\ &\equiv \frac{1}{2\pi}\sum_{n=\text{even}} e^{-in\zeta am_\eta v}\tilde{\varphi}(na), \end{aligned} \tag{39}$$

and

$$\begin{aligned}q_\eta(x,v) &\to \frac{a}{4\pi}\sum_z e^{-iz\zeta m_\eta v}\langle \eta(0)|(\psi_e^\dagger(-z)+\psi_o^\dagger(-z))e^{-i2vz\mathbb{H}}(\psi_e(+z)+\psi_o(+z))|\eta(0)\rangle \\ &= \frac{1}{2\pi}\sum_{n=\text{even}} e^{-in\zeta am_\eta v}\langle \eta(0)|(\varphi_{-n}^\dagger+\varphi_{-n+1}^\dagger)e^{-i2vn\mathbb{H}}(\varphi_{+n}+\varphi_{+n+1})|\eta(0)\rangle \\ &\equiv \frac{1}{2\pi}\sum_{n=\text{even}} e^{-in\zeta am_\eta v}\tilde{D}(na). \end{aligned} \tag{40}$$

In Fig. 7 (left) we show the numerical results for the spatial parton distributions by exact diagonalization using the "time" evolved form (39). We fixed $v = 1$ and $m/m_s = 0.1$ using the improved lattice mass (33), and $N = 24$. The real part of the spatial distribution function $\text{Re}(\tilde{\text{D}}(\text{z}))$ and amplitude $\text{Re}(\tilde{\varphi}(\text{z}))$ (red marks) are compared to the exact inverse Fourier transforms before scaling (dashed lines), and after scaling by $\frac{1}{2}$ in z (brown-solid line).

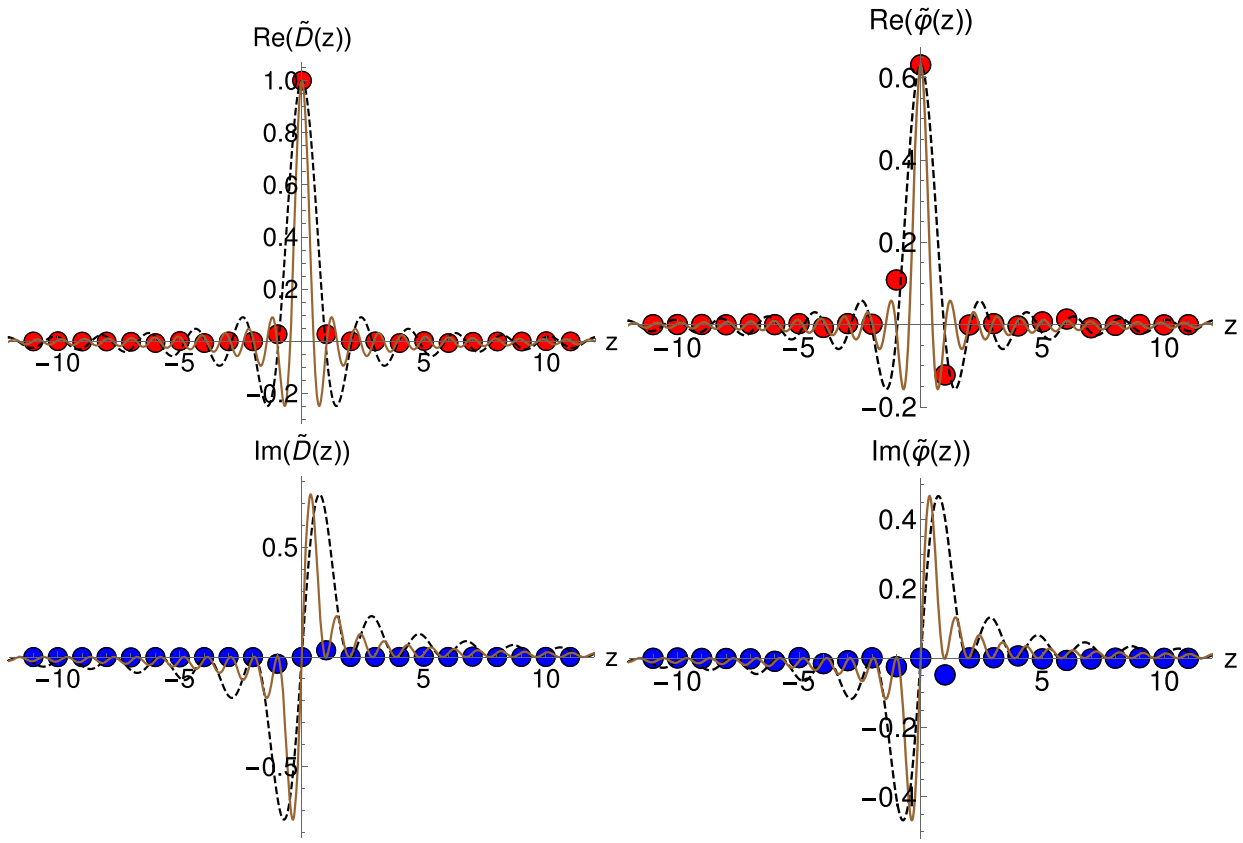

FIG. 7. Real (red) and imaginary (blue) part of $\tilde{D}(z)$ and $\varphi(z)$ for $v = 1$ and $m/m_s = 0.1$ using the improved mass, and the time-evolved form. The black dashed line is the inverse Fourier transform (normalized to the peak of the real part) of the solution to (B1). The brown line is the same function rescaled by $1/2$ in z. In the right panel, we used the arbitrary phase between $\langle 0|$ and $|\eta\rangle$ to impose that the imaginary part vanishes for $z = 0$. We fixed $N = 24$, $a = 1$ and the results are in units of $g = 1$.

In Fig. 7 (right) the imaginary part of the spatial distribution function $\mathrm{Im}(\tilde{\mathrm{D}}(\mathrm{z}))$ and amplitude $\mathrm{Im}(\tilde{\varphi}(\mathrm{z}))$ (blue marks) are compared to the inverse Fourier transforms before scaling (dashed lines), and after scaling by $\frac{1}{2}$ in z (brown-solid line).

The numerical results for the "time" evolved distributions, compare poorly to the exact results, in contrast to the boosted results presented earlier. The reason maybe traced to the use of the Hamiltonian in the "time" evolved form which is seen to scale extensively with N, a major source of oscillations and therefore uncertainty in the spatial distributions. This is not the case for the boost operator.

VII. CONCLUSIONS

We have solved massive two-dimensional QED on a discrete lattice of qubits by exact diagonalization, to analyze the quasiparton distributions of the lowest meson state, both at strong and weak coupling. The digitization is performed using the standard Jordan-Wigner map of the Kogut-Susskind fermions, in a spatial lattice with open boundary conditions. Our largest lattice consisted of $N = 24$ qubits following the mapping onto the spin system.

The boosted meson state is an eigenstate of both the Hamiltonian and momentum operators in the continuum with the proper relativistic kinematics independent of the rapidity. This is not the case for the numerically obtained first excited state of our system where increasingly large deviations from relativistic kinematics are manifest in the luminal limit.

The numerical results for the spatial quasidistribution functions and amplitudes obtained from exact diagonalization are relatively sparse for the largest number of qubits. This is the case for both the boosted and "time" evolved quasi-distributions. The latter are exactly the light cone distributions in the luminal case. When compared to the exact inverse Fourier transformed spatial quasidistribution functions and amplitudes, the results show overall consistency but are far from being accurate. This is expected due to the fairly large lattice spacing.

The numerical results for the "time" evolved spatial parton distribution function and amplitude are much less accurate than those obtained using the boosted form. This maybe traced to the large argument of the exponential in the "time" evolved form, where the Hamiltonian is seen to scale with the number of qubits, a major source of

oscillations and therefore uncertainty. This is not the case of the boost operator, which is less noisy since the lattice coordinate is in the weighted sum.

This exploratory analysis shows that the deviation from relativistic kinematics of the boosted hadronic states are visible already at moderately small rapidities and affect their orthonormality (due to finite size effects). More importantly, the oscillatory character of the spatial quasi-distribution functions, make them very hard to capture on a finite lattice. To improve on this, would require much finer lattices with many more qubits than we have used. Therefore, the results are encouraging and finer lattices, perhaps achieved through the use of tensor networks [54] or a computation on a quantum computer, could yield good agreement with the exact results. Our approach readily extends to the analysis of quasigeneralized parton distributions in massive QED2. We plan to address some of these issues in upcoming work.

ACKNOWLEDGMENTS

We thank Yahui Chai, Adrien Florio, and David Frenklakh for useful discussions. This work is supported by the Office of Science, U.S. Department of Energy under Contract No. DE-FG-88ER40388 (S. G., I. Z.). This research is also supported in part within the framework of the Quark-Gluon Tomography (QGT) Topical Collaboration, under Contract No. DE-SC0023646. The work of S. G. and K. I. was supported by the U.S. Department of Energy, Office of Science, National Quantum Information Science Research Centers, Co-design Center for Quantum Advantage (C2QA) under Contract No. DE-SC0012704. S. G. was in part supported by a Feodor Lynen Research fellowship of the Alexander von Humboldt foundation.

APPENDIX A: LF WAVE FUNCTIONS IN QED2

The numerical solutions to the eigenintegral (B1) were developed in [42], by expanding in a complete light front basis, which we summarize here for completeness. More specifically, we seek

$$\varphi(\zeta)=\sum_n c_n f_n(\zeta), \tag{A1}$$

as an expansion using orthonormal Jacobi polynomials,

$$f_n(\zeta)=C_n\left(\frac{1-\zeta^2}{4}\right)^{\beta}P_n^{(2\beta,2\beta)}(\zeta), \tag{A2}$$

with the normalization,

$$C_n=\left(\frac{n!}{2}(1+2n+4\beta)\frac{\Gamma(1+n+4\beta)}{\Gamma^2(1+n+2\beta)}\right)^{\frac{1}{2}}.$$

The first Jacobi polynomial is constant $P_0(\zeta)=1$, which leads the solution $f_0(\zeta)$ of the form (6). This suggests that only few terms in the expansion are needed. The variational parameter β is optimally fixed by minimizing the energy. Here, we will follow [42] and choose $\beta=\sqrt{3/\pi}(m/m_s)$ for sufficiently strong coupling.

In the basis set (A2), (B1) takes a matrix form,

$$(\mathbb{A}_{mn}+\mathbb{B}_{mn}+\mathbb{C}_{mn})c_n=\mu^2 c_m, \tag{A3}$$

$$\begin{aligned}\mathbb{A}_{mn}&=\frac{1}{2}\int_{-1}^{1}d\zeta d\zeta' f_m(\zeta)f_n(\zeta'),\\ \mathbb{B}_{mn}&=4\alpha\int_{-1}^{1}d\zeta\frac{f_m(\zeta)f_n(\zeta)}{(1-\zeta^2)},\\ \mathbb{C}_{mn}&=-2\mathrm{PP}\int_{-1}^{1}d\zeta d\zeta'\frac{f_m(\zeta)(f_n(\zeta')-f_n(\zeta))}{(\zeta-\zeta')^2}.\end{aligned} \tag{A4}$$

Note that the entries $\mathbb{A}_{mn}$ in (A3) is what distinguish the massive Schwinger equation from the 't Hooft equation. It is due to the U(1) anomaly in QED2.

APPENDIX B: X-REPRESENTATION

The solutions in the x-representation with

$$x=\frac{1+\zeta}{2}\qquad \bar{x}=1-x=\frac{1-\zeta}{2}$$

valued in $0\le x,\bar{x}\le 1$, follow from

$$\mu^2\varphi(x)=\int_0^1 dy\,\varphi(y)+\frac{\alpha}{x\bar{x}}\varphi(x)-\mathrm{PP}\int_0^1 dy\frac{\varphi(y)-\varphi(x)}{(x-y)^2}. \tag{B1}$$

In this representation, the basis expansion is

$$\varphi(x)=\sum_n \bar{c}_n\bar{f}_n(x), \tag{B2}$$

with

$$\bar{f}_n(x)=\bar{C}_n(x\bar{x})^{\beta}P_n^{(2\beta,2\beta)}(x-\bar{x}). \tag{B3}$$

Moreover, the normalization is given by

$$\bar{C}_n=\left(n!(1+2n+4\beta)\frac{\Gamma(1+n+4\beta)}{\Gamma^2(1+n+2\beta)}\right)^{\frac{1}{2}}.$$

The matrix form of (B1) is

$$(\bar{\mathbb{A}}_{mn}+\bar{\mathbb{B}}_{mn}+\bar{\mathbb{C}}_{mn})\bar{c}_n=\mu^2\bar{c}_m, \tag{B4}$$

with the matrix entries

$$\bar{\mathbb{A}}_{mn} = \int_0^1 dxdy\, \bar{f}_m(x)\bar{f}_n(y), \tag{B5}$$

$$\bar{\mathbb{B}}_{mn} = \alpha \int_0^1 dx \frac{\bar{f}_m(x)\bar{f}_n(x)}{x\bar{x}}, \tag{B6}$$

$$\bar{\mathbb{C}}_{mn} = -\mathrm{PP}\int_0^1 dxdy \frac{\bar{f}_m(x)(\bar{f}_n(y) - \bar{f}_n(x))}{(x-y)^2}. \tag{B7}$$

To perform the integrals analytically, we note the identity [55],

$$\mathrm{PP}\int_0^1 dxdy \frac{(x\bar{x})^\alpha (y\bar{y})^\beta}{(x-y)^2} = -\frac{2\pi}{2^{2(\alpha+\beta)}} \frac{\alpha\beta\Gamma(\alpha)\Gamma(\beta)}{(\alpha+\beta)\Gamma\left(\alpha+\frac{1}{2}\right)\Gamma\left(\beta+\frac{1}{2}\right)}. \tag{B8}$$

We also note that since the distribution amplitudes,

$$\varphi(-\zeta) = \pm\varphi(\zeta),$$

have fixed "parity," the contributions to (B2) stem from either even or odd Jacobi Polynomials. For the even polynomials,

$$P_{2n}^{2\beta,2\beta}(x-\bar{x}) = \sum_{m=0}^{n}\sum_{k=0}^{m}\binom{m}{k} a_m(-4x\bar{x})^k, \tag{B9}$$

is a polynomial in $x\bar{x}$, while for the odd polynomials behave as

$$P_{2n+1}^{2\beta,2\beta}(x-\bar{x}) = \sum_{m=0}^{n}\sum_{k=0}^{m}\binom{m}{k} a_m(2x-1)(-4x\bar{x})^k. \tag{B10}$$

These observations, combined with (B8) allow us to evaluate all matrix entries in (B5) in closed analytical form. Note that in the x-representation, the parton distribution amplitude is

$$q_\eta(x) = |\varphi(x)|^2. \tag{B11}$$

[1] R. Abdul Khalek *et al.*, Science requirements and detector concepts for the electron-ion collider: EIC Yellow Report, Nucl. Phys. **A1026**, 122447 (2022).
[2] Raktim Abir *et al.*, The case for an EIC theory alliance: Theoretical challenges of the EIC, arXiv:2305.14572.
[3] Xiangdong Ji, Parton physics on a euclidean lattice, Phys. Rev. Lett. **110**, 262002 (2013).
[4] Jian-Hui Zhang, Jiunn-Wei Chen, Xiangdong Ji, Luchang Jin, and Huey-Wen Lin, Pion distribution amplitude from lattice QCD, Phys. Rev. D **95**, 094514 (2017).
[5] Xiangdong Ji, Andreas Schäfer, Xiaonu Xiong, and Jian-Hui Zhang, One-loop matching for generalized parton distributions, Phys. Rev. D **92**, 014039 (2015).
[6] Gunnar S. Bali, Vladimir M. Braun, Benjamin Gläßle, Meinulf Göckeler, Michael Gruber, Fabian Hutzler, Piotr Korcyl, Andreas Schäfer, Philipp Wein, and Jian-Hui Zhang, Pion distribution amplitude from Euclidean correlation functions: Exploring universality and higher-twist effects, Phys. Rev. D **98**, 094507 (2018).
[7] Constantia Alexandrou, Krzysztof Cichy, Martha Constantinou, Karl Jansen, Aurora Scapellato, and Fernanda Steffens, Transversity parton distribution functions from lattice QCD, Phys. Rev. D **98**, 091503 (2018).
[8] Taku Izubuchi, Luchang Jin, Christos Kallidonis, Nikhil Karthik, Swagato Mukherjee, Peter Petreczky, Charles Shugert, and Sergey Syritsyn, Valence parton distribution function of pion from fine lattice, Phys. Rev. D **100**, 034516 (2019).
[9] Taku Izubuchi, Xiangdong Ji, Luchang Jin, Iain W. Stewart, and Yong Zhao, Factorization theorem relating Euclidean and light-cone parton distributions, Phys. Rev. D **98**, 056004 (2018).
[10] Raúl A. Briceño, Maxwell T. Hansen, and Christopher J. Monahan, Role of the Euclidean signature in lattice calculations of quasidistributions and other nonlocal matrix elements, Phys. Rev. D **96**, 014502 (2017).
[11] Anatoly V. Radyushkin, Pion distribution amplitude and quasi-distributions, Phys. Rev. D **95**, 056020 (2017).
[12] Yan-Qing Ma and Jian-Wei Qiu, Extracting parton distribution functions from lattice QCD calculations, Phys. Rev. D **98**, 074021 (2018).
[13] Xiangdong Ji, Yizhuang Liu, and Ismail Zahed, Quasiparton distribution functions: Two-dimensional scalar and spinor QCD, Phys. Rev. D **99**, 054008 (2019).
[14] Tianyin Li, Xingyu Guo, Wai Kin Lai, Xiaohui Liu, Enke Wang, Hongxi Xing, Dan-Bo Zhang, and Shi-Liang Zhu (QuNu Collaboration), Partonic collinear structure by quantum computing, Phys. Rev. D **105**, L111502 (2022).
[15] Tianyin Li, Xingyu Guo, Wai Kin Lai, Xiaohui Liu, Enke Wang, Hongxi Xing, Dan-Bo Zhang, and Shi-Liang Zhu (QuNu Collaboration), Exploring light-cone distribution amplitudes from quantum computing, Sci. China Phys. Mech. Astron. **66**, 281011 (2023).
[16] Henry Lamm, Scott Lawrence, and Yukari Yamauchi (NuQS Collaboration), Parton physics on a quantum computer, Phys. Rev. Res. **2**, 013272 (2020).
[17] Adrián Pérez-Salinas, Juan Cruz-Martinez, Abdulla A. Alhajri, and Stefano Carrazza, Determining the proton content with a quantum computer, Phys. Rev. D **103**, 034027 (2021).

[18] Raúl A. Briceño, Juan V. Guerrero, Maxwell T. Hansen, and Alexandru M. Sturzu, Role of boundary conditions in quantum computations of scattering observables, Phys. Rev. D **103**, 014506 (2021).
[19] Michael Kreshchuk, William M. Kirby, Gary Goldstein, Hugo Beauchemin, and Peter J. Love, Quantum simulation of quantum field theory in the light-front formulation, Phys. Rev. A **105**, 032418 (2022).
[20] M. G. Echevarria, I. L. Egusquiza, E. Rico, and G. Schnell, Quantum simulation of light-front parton correlators, Phys. Rev. D **104**, 014512 (2021).
[21] John B. Kogut and Leonard Susskind, Hamiltonian formulation of Wilson's lattice gauge theories, Phys. Rev. D **11**, 395 (1975).
[22] Leonard Susskind, Lattice fermions, Phys. Rev. D **16**, 3031 (1977).
[23] Pascual Jordan and Eugene P. Wigner, About the Pauli exclusion principle, Z. Phys. **47**, 631 (1928).
[24] Douglas Beck *et al.*, Quantum information science and technology for nuclear physics. Input into U.S. long-range planning, 2023, arXiv:2303.00113.
[25] M. Fannes, B. Nachtergaele, and R. F. Werner, Finitely correlated states on quantum spin chains, Commun. Math. Phys. **144**, 443 (1992).
[26] Stefan Rommer and Stellan Östlund, Class of ansatz wave functions for one-dimensional spin systems and their relation to the density matrix renormalization group, Phys. Rev. B **55**, 2164 (1997).
[27] Stellan Östlund and Stefan Rommer, Thermodynamic limit of density matrix renormalization, Phys. Rev. Lett. **75**, 3537 (1995).
[28] Steven R. White, Density matrix formulation for quantum renormalization groups, Phys. Rev. Lett. **69**, 2863 (1992).
[29] U. Schollwöck, The density-matrix renormalization group, Rev. Mod. Phys. **77**, 259 (2005).
[30] Roland C. Farrell, Marc Illa, Anthony N. Ciavarella, and Martin J. Savage, Scalable circuits for preparing ground states on digital quantum computers: The Schwinger model vacuum on 100 qubits, PRX Quantum **5**, 020315 (2024).
[31] Roland C. Farrell, Marc Illa, Anthony N. Ciavarella, and Martin J. Savage, Quantum simulations of hadron dynamics in the Schwinger model using 112 qubits, Phys. Rev. D **109**, 114510 (2024).
[32] Adrien Florio, David Frenklakh, Kazuki Ikeda, Dmitri E. Kharzeev, Vladimir Korepin, Shuzhe Shi, and Kwangmin Yu, Quantum simulation of entanglement and hadronization in jet production: Lessons from the massive Schwinger model, arXiv:2404.00087.
[33] Ross Dempsey, Igor R. Klebanov, Silviu S. Pufu, and Bernardo Zan, Discrete chiral symmetry and mass shift in the lattice Hamiltonian approach to the Schwinger model, Phys. Rev. Res. **4**, 043133 (2022).
[34] M. C. Bañuls, K. Cichy, K. Jansen, and J. I. Cirac, The mass spectrum of the Schwinger model with matrix product states, J. High Energy Phys. 11 (2013) 158.
[35] Boye Buyens, Jutho Haegeman, Karel Van Acoleyen, Henri Verschelde, and Frank Verstraete, Matrix product states for gauge field theories, Phys. Rev. Lett. **113**, 091601 (2014).
[36] Julian S. Schwinger, Gauge invariance and mass. 2. Phys. Rev. **128**, 2425 (1962).
[37] Sidney R. Coleman, More about the massive Schwinger model, Ann. Phys. (N.Y.) **101**, 239 (1976).
[38] Sebastian Grieninger, Kazuki Ikeda, Dmitri E. Kharzeev, and Ismail Zahed, Entanglement in massive Schwinger model at finite temperature and density, Phys. Rev. D **109**, 016023 (2024).
[39] Ivo Sachs and Andreas Wipf, Finite temperature Schwinger model, Helv. Phys. Acta **65**, 652 (1992).
[40] James V. Steele, J. J. M. Verbaarschot, and I. Zahed, The invariant fermion correlator in the Schwinger model on the torus, Phys. Rev. D **51**, 5915 (1995).
[41] Hugh Bergknoff, Physical particles of the massive Schwinger model, Nucl. Phys. **B122**, 215 (1977).
[42] Yi-zhang Mo and Robert J. Perry, Basis function calculations for the massive Schwinger model in the light front Tamm-Dancoff approximation, J. Comput. Phys. **108**, 159 (1993).
[43] Gerard 't Hooft, A two-dimensional model for mesons, Nucl. Phys. **B75**, 461 (1974).
[44] Roman Zubov and Evgeni Prokhvatilov, On numerical solutions to the QCD 't Hooft equation in the limit of large quark mass, AIP Conf. Proc. **1701**, 100001 (2016).
[45] Tom Banks, Leonard Susskind, and John B. Kogut, Strong coupling calculations of lattice gauge theories: $(1+1)$-dimensional exercises, Phys. Rev. D **13**, 1043 (1976).
[46] Oscar Higgott, Daochen Wang, and Stephen Brierley, Variational quantum computation of excited states, Quantum **3**, 156 (2019).
[47] Dmitri E. Kharzeev and Yuta Kikuchi, Real-time chiral dynamics from a digital quantum simulation, Phys. Rev. Res. **2**, 023342 (2020).
[48] Wibe A. de Jong, Kyle Lee, James Mulligan, Mateusz Płoskoń, Felix Ringer, and Xiaojun Yao, Quantum simulation of nonequilibrium dynamics and thermalization in the Schwinger model, Phys. Rev. D **106**, 054508 (2022).
[49] Kazuki Ikeda, Dmitri E. Kharzeev, and Yuta Kikuchi, Real-time dynamics of Chern-Simons fluctuations near a critical point, Phys. Rev. D **103**, L071502 (2021).
[50] Adrien Florio, David Frenklakh, Kazuki Ikeda, Dmitri Kharzeev, Vladimir Korepin, Shuzhe Shi, and Kwangmin Yu, Real-time nonperturbative dynamics of jet production in Schwinger model: Quantum entanglement and vacuum modification, Phys. Rev. Lett. **131**, 021902 (2023).
[51] Kazuki Ikeda, Dmitri E. Kharzeev, René Meyer, and Shuzhe Shi, Detecting the critical point through entanglement in the Schwinger model, Phys. Rev. D **108**, L091501 (2023).
[52] João Barata, Wenjie Gong, and Raju Venugopalan, Realtime dynamics of hyperon spin correlations from string fragmentation in a deformed four-flavor Schwinger model, Phys. Rev. D **109**, 116003 (2024).
[53] Ross Dempsey, Igor R. Klebanov, Silviu S. Pufu, and Bernardo Zan, Discrete chiral symmetry and mass shift in the lattice Hamiltonian approach to the Schwinger model, Phys. Rev. Res. **4**, 043133 (2022).
[54] Adrien Florio, Two-fermion negativity and confinement in the Schwinger model, Phys. Rev. D **109**, L071501 (2024).
[55] William A. Bardeen, Robert B. Pearson, and Eliezer Rabinovici, Hadron masses in quantum chromodynamics on the transverse lattice, Phys. Rev. D **21**, 1037 (1980).